Developing New Sustainable Pyridinium Ionic Liquids: From Reactivity Studies to Mechanism-Based Activity Predictions

Bakhtiyor Borikhonov
Karshi State University
Elyor Berdimurodov (elyor170690@gmail.com)
National University of Uzbekistan https://orcid.org/0000-0003-0610-8218
Tursunali Kholikov
National University of Uzbekistan named after Mirzo Ulugbek
Konstantin P. Katin
MEPhI: Nacional'nyj issledovatel'skij adernyj universitet Moskovskij inzenerno-fiziceskij institut
Muslum DEMİR
Osmaniye Korkut Ata Universitesi
Frunza Sapaev
National University of Uzbekistan named after Mirzo Ulugbek
Sherzod Turaev
National University of Uzbekistan named after Mirzo Ulugbek
Nigora Jurakulova
Karshi State University

Research Article

Keywords: Pyridinium ionic liquids, Structure-activity relationships, Plant growth promotion, Herbicidal activity, Insecticidal activity, Computational drug design

Posted Date: October 10th, 2023

DOI: https://doi.org/10.21203/rs.3.rs-3398070/v1

Developing New Sustainable Pyridinium Ionic Liquids: From Reactivity Studies to Mechanism-Based Activity Predictions

Bakhtiyor Borikhonov[1], Elyor Berdimurodov[2,3,4]*, Tursunali Kholikov[4], Konstantin P. Katin[5], Muslum DEMİR[6,7], Frunza Sapaev[4], Sherzod Turaev[4], Nigora Jurakulova[1]

[1]Faculty of Chemistry-Biology, Karshi State University, Karshi, 130100, Uzbekistan.
[2]Chemical & Materials Engineering, New Uzbekistan University, 54 Mustaqillik Ave., Tashkent, 100007, Uzbekistan.
[3]Akfa University, Milliy Bog' Street 264, Tashkent, 111221, Uzbekistan.
[4]Faculty of Chemistry, National University of Uzbekistan, Tashkent, 100034, Uzbekistan.
[5]National Research Nuclear University "MEPhI", Kashirskoe Shosse 31, Moscow, 115409, Russian Federation.
[6]TUBITAK Marmara Research Center, Material Institute, Gebze 41470, Turkey.
[7]Osmaniye Korkut Ata University, Osmaniye 80000, Turkey.

Abstract

Recently, pyridinium-based ionic liquids have been received great attention thanks to their unique features, such as low melting points, low volatility, high thermal stability, and moderate solvation properties. In the present work, for the first time, three pyridinium-based ionic liquids 1-(2-(isopentyloxy)-2-oxoethyl)pyridin-1-ium chloride, 1-(2-(hexyloxy)-2-oxoethyl)pyridin-1-ium chloride, and 1-(2-(benzyloxy)-2-oxoethyl)pyridin-1-ium chloride were synthesized by simply reacting pyridine with esters of monochloroacetic acid. The biological activities of as-prepared compounds were evaluated experimentally through plant growth promotion, herbicidal, and insecticidal assays The biological test results show thate benzyloxy derivative stimulated wheat and cucumber growth over 20% at lower doses. The isopentyloxy compound was the most effective herbicide, reducing root/stem growth by >80%.. To support experimental data, the computational methods including DFT calculations, molecular docking and druglikeness prediction were also applied. It was found that the benzyloxy salt had the highest predicted binding affinities and druglikeness and yield was for pure salt production is in 78-86%. An integrated experimental-computational approach provided insights into structure-activity relationships and mechanisms of action. The results showed the biological activity depends on substituent chain length/structure, influencing lipophilicity and membrane/target interactions. The findings support further development of optimized pyridinium ionic liquids as natural active agents for agriculture and pharmaceutical applications. These ionic salts are suggested as potential agent in agricultural, pharmaceutical and industrial application.

Keywords: Pyridinium ionic liquids; Structure-activity relationships; Plant growth promotion; Herbicidal activity; Insecticidal activity; Computational drug design.

1. Introduction

Ionic liquids (ILs) are organic salts with melting points below 100°C that exhibit desirable properties such as low volatility, non-flammability, and good solvation capabilities. Ionic liquids (ILs) are organic salts with melting points below 100°C that exhibit desirable properties such as low volatility, non-flammability, and good solvation capabilities. Ionic Liquids (ILs) have garnered significant attention for their diverse applications in green chemistry, catalysis, separations, and, more recently, as biologically active agents [1-4]. Conventional ILs typically consist of imidazolium, pyridinium, or ammonium cations paired with halide, sulfonate, or other anions. Nonetheless, the exploration of alternative ionic structures still going on to enhance physical and chemical characteristics of ILs. Quaternary ammonium salts represent a subclass of ILs distinguished by a tetra-substituted ammonium cation. The previous studies proved that the organic substituents notably affect biological activity [5-8]. In other word, the quaternary ammonium compounds (QACs) exhibit antimicrobial, herbicidal, and plant growth regulatory properties attributed to their cationic charge and hydrophobic domains. Nevertheless, the rational design of new QACs with well-defined structure-activity relationships (SARs) remains an ongoing challenge [9-12].

Conventional ILs typically involve cations based on imidazolium, pyridinium, or ammonium, paired with inorganic or organic anions. Nevertheless, the exploration of novel cation and anion combinations remains an active research endeavor aimed at discovering ILs with tailored physicochemical characteristics

and specialized functions. Quaternary ammonium salts represent one important subclass of ILs, characterized by a tetra-substituted ammonium cation. The organic substituents attached to the central nitrogen atom can be systematically modified to adjust physical and electronic properties and introduce biological activities [13-16]. Prior studies have demonstrated that quaternary ammonium compounds (QACs) possess potent antibacterial, antifungal, and herbicidal properties due to their cationic charge and hydrophobic functionalities. These cationic surfactants are believed to interact with and disrupt microbial and plant cell membranes. Structural modifications affecting lipophilicity, hydrogen bonding, and steric effects can influence selectivity between membranes and intracellular targets [17-20]. Consequently, there is a growing interest in developing environmentally-friendly agrochemicals, disinfectants, and pharmaceuticals, with rationally-designed ILs offering a sustainable approach as biodegradable active ingredients. While much attention has been devoted to imidazolium and ammonium ILs, pyridinium salts represent an underexplored class with potential for biological applications [21-24]. The reactivity of pyridine allows for facile synthesis and structure-activity relationship (SAR) studies due to its weaker basicity compared to aliphatic amines. Previous computational investigations have employed methods such as density functional theory (DFT) calculations, quantitative structure-activity relationships (QSAR) modeling, and molecular docking to examine ionic liquid structures, reactivity, and mechanisms of action. However, an integrated experimental-computational approach is required to comprehensively elucidate SARs and guide new designs [25-29].

In this study, we present the synthesis, characterization, and evaluation of novel pyridinium-based ionic liquids as potential biologically active agents. We prepared three quaternary ammonium salts by reacting pyridine with different esters of monochloroacetic acid. The structures were analyzed using infrared spectroscopy and NMR techniques. Subsequently, biological assays assessed their growth-promoting, herbicidal, and insecticidal effects across a range of plant and pest models. Computational methods, including density functional theory (DFT) calculations, molecular docking, and druglikeness prediction, were also applied to gain insights into electronic properties, binding interactions, and mechanisms of action. Overall, this integrated experimental-computational study aims to provide valuable SAR knowledge for the rational design of next-generation natural ILs as agrochemical and pharmaceutical leads.

2. Materials and methods

2.1.Materials

Pyridine (99%), hexanol (99%), benzyl alcohol (99%), monochloroacetic acid (97%), 3-methyl-pentanol (98%), ethyl acetate (99%), ethanol (96%), acetone (99%) were purchased from Sigma-Aldrich.

Methods

Synthesis of Quaternary Ammonium Salts

The appropriate ester of monochloroacetic acid (2 mol) was added to a solution of pyridine (1 mol) in ethanol (10 mL). The reaction mixture was heated at 50-60°C for 3 hours. Upon completion, the reaction solvent was removed under reduced pressure. The residue was recrystallized from ethanol to obtain the pure quaternary ammonium salt product.

Structural Analysis

Infrared Spectroscopy (IR)

IR spectra were obtained on a SPECORD-75IR spectrophotometer using KBr discs.

Nuclear Magnetic Resonance (NMR) Spectroscopy

^{1}H NMR spectra were recorded on a Unity 400plus spectrometer operating at 400 MHz for ^{1}H. Deuterated methanol (CD_3OD) was used as the solvent and hexamethyldisiloxane (HMDSO) as the internal standard.

2.2. Research methodology in biological activity

Growth-promoting activity

To assess growth-promoting activity, wheat and cucumber seeds were germinated under controlled environmental conditions. Solutions of the test quaternary ammonium salts ranging from 0.0001-0.1% concentration as well as a Floroxan positive control at 0.00001% were prepared. Seeds were treated with 200 μL of each solution or a water control. After a set growth period, seedling root length, stem height, and growth percentages compared to controls were measured. Each treatment was replicated four times and the results were reported as means.

Herbicidal activity

For evaluating herbicidal activity, wheat and cucumber seeds were planted in soil in a growth chamber. Solutions of the test compounds from 0.0001-0.1% and herbicide standards Fusilade and Stomp were prepared. Plant foliage was sprayed with 200 μL of each solution at the defined concentrations. Seedling root and stem development was then assessed and growth inhibition percentages compared to controls were determined. Each treatment was replicated four times to obtain average results.

Insecticidal activity

To test insecticidal activity, C. maculatus insects were reared under controlled temperature and lighting conditions for use in bioassays. Test compound solutions ranging from 1-0.01% along with a BAGIRA control from 0.1-0.01% were prepared. Petri dishes were treated with 200 μL doses and 20 insects per dish. Mortality was recorded at 24 hours and biological activity was calculated using Abbott's formula. Each treatment was replicated four times and results were expressed as the mean mortality percentage.

This ensured consistent and quantifiable evaluation of the various biological activities of the novel compounds.

Computational details

It was combined the dispersion-corrected density functional theory (DFT) with molecular docking study and Petra/Osiris/Molinspiration (POM) analysis to investigate structures and biological activities of three considered molecules. Optimal geometries of all molecules were found with the B3LYP exchange-corrected functional [30, 31] and 6-311G** electronic basis set [32]. Grimme's D3 corrections were taken into account [33]. GAMESS-US software were used for all DFT calculations [34]. Ionization potential (IP) and electron affinity (EA) were derived from frontier molecular orbitals HOMO and LUMO according to empirical formulas based on the Koopmans's theorem [35]:

$$IP \approx -0.78 \cdot E_{HOMO} + 3.17; \; EA \approx -0.65 \cdot E_{LUMO} - 0.38.$$

After obtaining the IP and EA values, it was calculated quantum descriptors of reactivity, such as electronegativity (χ), chemical potential (μ), chemical hardness (η) and softness (S), electrophilicity (ω) and nucleophilicity (ε) indexes, electrodonating (ω^-) and electroaccepting (ω^+) powers. These descriptors were calculated with the well-known formulas [36, 37]:

$$\chi = (IP + EA)/2$$
$$\mu = -\chi$$
$$\eta = (IP - EA)/2$$
$$S = 1/(2\eta)$$
$$\omega = \mu^2 S$$
$$\varepsilon = 1/\omega$$
$$\omega^- = (3IP + EA)^2/(16(IP - EA))$$
$$\omega^+ = (IP + 3EA)^2/(16(IP - EA)).$$

To get additional insight about the biological activity of the considered molecules, we investigated their docking on some cancer-related proteins. For this purpose, we applied the CB-dock server based on popular AutoDock Vina software [38]. We also estimated the value of the association constant K_a for the ligand-protein docking. Although the calculated Vina score (VS) should not be identified with the Gibbs energy of the docking process, the K_a value can be roughly estimate from VS as it was described in [39]:

$$K_a\ (M^{-1}) \approx \exp\ (VS/RT).$$

Here $R = 1.987 \cdot 10^{-3}$ kcal/(mol·K) is the Boltzmann's constant, $T = 309.75$ K is the normal temperature of the human body.

It was also predicted the pharmaceutical potentials of the considered molecules with the Petra/Osiris/Molinspiration (POM) analysis, which is commonly applied to novel molecules, which can hypothetically be used as the drugs [40].

3. Results and discussion

3.1. Experimental part and spectroscopic analysis

1-(2-(Isopentyloxy)-2-oxoethyl)pyridin-1-ium chloride was obtained from the reaction between pyridine and 3-methyl-pentyl ester of monochloroacetic acid. The yield of 1-(2-(isopentyloxy)-2-oxoethyl)pyridin-1-ium chloride formed in the reaction is found to be 84% (5.11 g), mp. = 217 ^{0}C.

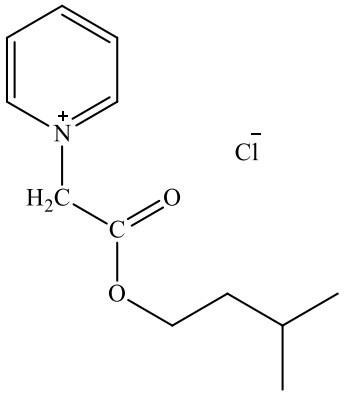

IR spectral analysis:

The broad bands between 3337-3160 cm^{-1} correspond to O-H and/or N-H stretching vibrations. The presence of hydrogen-bonding functional groups is indicated. The signals located at 3292 and 3012 cm^{-1} can be assigned to aliphatic C-H stretches from the isopentyl group. The absorbances placed at 1668, 1637, 1616 cm^{-1} are correspond to C=O stretching of the ester carbonyl and C=C/C=N stretches within the pyridinium ring. The peak observed at 1398 cm^{-1} represents C-N stretching, while the band at 1093 cm^{-1} involves C-O stretching of the ester linkage.

In the fingerprint region:

- The 766 cm^{-1} band corresponds to out-of-plane C-H bends.
- The 684 cm^{-1} peak is assigned to pyridinium ring deformation.
- The absorbance at 636 cm^{-1} indicates C-C-C bending of the isopentyl substituent.

Overall, the IR spectrum is consistent with the presence of the major functional groups expected in 1-(2-(isopentyloxy)-2-oxoethyl)pyridin-1-ium chloride, supporting its proposed structure (Figure 1S).

^{1}H NMR analysis:

The ^{1}H NMR spectrum shows prominent multiplets seen at 1.99 ppm and 2.01 ppm, each integrating to 6H. These signals correspond to the methyl protons (CH_3) of the isopentyl group. The multiplet at 1.99 ppm indicates the presence of vicinal (geminal + vicinal) coupling. Considering typical coupling constants:

- Geminal coupling ($J \approx 15$ Hz) between the two equivalent protons in the CH_3 group. This would appear as a doublet of doublets.
- Vicinal coupling ($J \approx 7$ Hz) to the adjacent methylene protons. This coupling would further split each line of the doublet of doublets into another doublet.

Together, the complex multiplet pattern observed at 1.99 ppm arises from the CH_3 protons experiencing both types of coupling. Similarly, the 2.01 ppm multiplet corresponds to another set of geminally/vicinally coupled CH_3 protons. The singlets observed at 3.849 ppm and 3.193 ppm indicate no vicinal/geminal couplings are present for these OCH_2 groups ($J \approx 0$ Hz). In summary, the complex multiplets at 1.99 and 2.01 ppm can be deconvoluted based on typical NMR coupling constants, fully supporting the assigned structure with two vicinally coupled isopentyl CH_3 environments (Figure 2S).

1-(2-(Hexyloxy)-2-oxoethyl)pyridin-1-ium chloride was obtained from the reaction of pyridine with hexyl ester of monochloroacetic acid. The product yield is calculated as 80% (2.57 g). mp.= 211 ^{0}C.

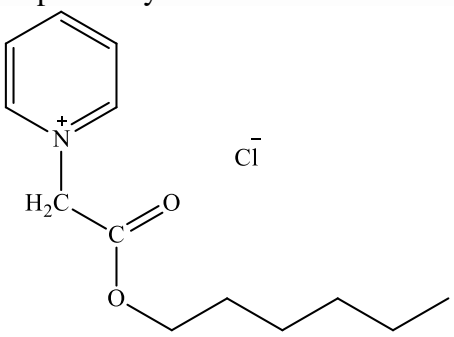

IR spectral analysis:

The bands at 3066 and 3336 cm^{-1} can be assigned to aromatic C-H stretches from the benzyl ring. The peaks between 2573-2407 cm^{-1} correspond to O-H or N-H stretches, indicative of hydrogen bonding. The strong absorbance at 1726 cm^{-1} is attributed to the carbonyl C=O stretch of the ester group. The band at 1636 cm^{-1} represents aromatic C=C stretching vibrations within the benzyl ring. The peak at 1490 cm^{-1}

involves C-C stretches of the benzene ring. The signal at 1398 cm^{-1} corresponds to C-N stretching of the pyridinium moiety (Figure 3S).

In the fingerprint region:

- 1199 cm^{-1} = C-O-C ester asymmetric stretch
- 818, 779 cm^{-1} = aromatic C-H out-of-plane bending
- 694 cm^{-1} = pyridinium ring deformation

Overall, the IR data is consistent with the expected functional groups of 1-(2-(benzyloxy)-2-oxoethyl)pyridin-1-ium chloride like the ester carbonyl, pyridinium, benzyl ring and hydrogen bonding motifs.

^{1}H NMR analysis:

The multiplet at 0.78 ppm integrating to 5H corresponds to the CH_3 protons. It shows (Figure 4S):

- Geminal coupling ($J \approx 15$ Hz) within the CH_3 group
- Vicinal coupling ($J \approx 7$ Hz) to the adjacent CH_2 group

The multiplet at 2.44 ppm integrating to 6H represents the methylene (CH_2) protons adjacent to the benzyl group. It involves similar geminal and vicinal coupling patterns. The doublet at 4.85 ppm integrating to 2H is assigned to the benzyl CH_2 protons. The splitting indicates:

- Vicinal coupling ($J \approx 15$ Hz) to the neighboring methylene protons

The multiplets at 7.45 ppm and 3.38 ppm integrating to 5H and 4H respectively correspond to the aromatic and glycyl methylene protons. In summary, the observed splitting patterns are fully consistent with the expected geminal and vicinal coupling interactions between the aliphatic and benzyl ring proton environments in the proposed structure. This analysis supports the identity and purity of the synthesized compound.

1-(2-(Benzyloxy)-2-oxoethyl)pyridin-1-ium chloride was obtained from the reaction of pyridine with benzyl ester of monochloroacetic acid. The product yield is measured as 81% (2.66 g). mp. = 209 ^{0}C.

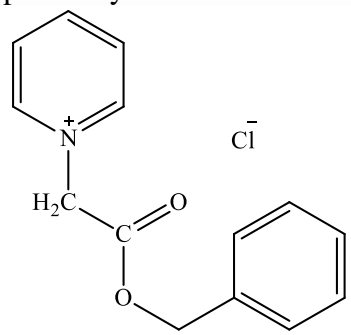

IR spectral analysis:

The broad bands between 3664-3130 cm^{-1} correspond to O-H/N-H stretching vibrations, suggesting hydrogen bonding. The peaks at 2962, 2897 cm^{-1} are attributed to C-H stretches of the aliphatic methylene groups. The signals at 1492, 1456 cm^{-1} involve aromatic C=C stretches of the benzene ring. The band at 1396 cm^{-1} corresponds to C-N stretching of the pyridinium moiety (Figure 5S).

In the fingerprint region:

- 989 cm^{-1} = C-O-C asymmetric stretch of the ester
- 854, 815 cm^{-1} = aromatic C-H out-of-plane bends
- 777, 731 cm^{-1} = pyridinium ring deformation
- 704, 669 cm^{-1} = methylene C-H bends
- 459 cm^{-1} = C-C stretches

Overall, the IR absorptions are consistent with the key structural elements of 1-(2-(Benzyloxy)-2-oxoethyl)pyridin-1-ium chloride such as the ester, benzene ring, pyridinium and presence of hydrogen bonding. This supports the proposed identity of the synthesized compound.

^{1}H NMR analysis:

The multiplets at 1 ppm and 1.13 ppm integrate to 2H each, representing equivalent methylene environments (CH_2). The splitting suggests vicinal coupling ($J \approx 7$ Hz) between the protons (Figure 6S). The multiplets at 0.46 ppm and 0.5 ppm, integrating to 3H each, represent methyl groups (CH_3). They show geminal coupling ($J \approx 15$ Hz) and vicinal coupling ($J \approx 7$ Hz) to neighboring CH_2 protons. The complex multiplet at 2.05 ppm integrating to 7H corresponds to methylene (CH_2) protons vicinal to the benzyl group.

It involves geminal and vicinal couplings with J values of ≈15 Hz and 7 Hz respectively. The multiplet at 1.11 ppm integrating to 6H represents another methylene environment exhibiting similar complex coupling patterns. The signals at 2.66 ppm and 1.87 ppm integrate to aromatic and methylene protons respectively, with overlapping geminal/vicinal couplings evident in the splitting patterns. In summary, all observed 1H NMR spectroscopic data is fully consistent with the proposed structure, with each proton environment displaying the expected coupling behavior.

3.2. Synthesis methodology analysis: Reaction optimization

This research in depth-investigated the experimental optimization for a reaction between monochloroacetic acid esters and pyridine. These reactions are carried out to produce quaternary ammonium salts. Three distinct solvents, such as, ethanol, acetone, and ethyl acetate were used to carry out the reactions since solvents can alter the reaction rate, selectivity, and yield. According to the generic chemical reaction diagram in Figure 1, monochloroacetic acid esters (R) combine with pyridine to produce quaternary ammonium ions. Three particular esters: 3-methylpentyl (-C_5H_{11}), hexyl (-C_6H_{13}), and benzyl ($C_6H_5CH_2$-) were employed in the investigation. The synthesis of several quaternary ammonium salts by changing the ester group (R) and examining the effect of the solvent on the reaction were probably the main objectives of the aforementioned study. The results would give information about the ideal reaction conditions, which could direct subsequent attempts at synthesis and prospective uses for these molecules.

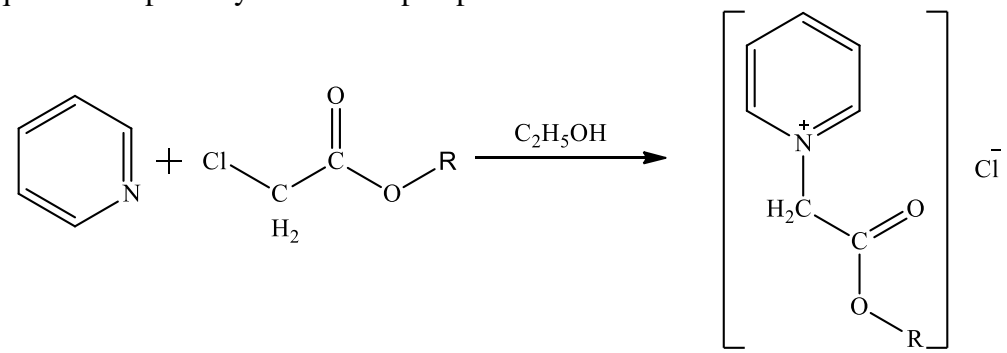

R = 3-Methyl-pentyl (-C_5H_{11}), Hexyl (-C_6H_{13}) and Benzyl $C_6H_5CH_2$-

Figure 1. General chemical reaction schema.

The results show the effect of temperature (30-40, 50-60, 80-90°C) on yield of reacting pyridine and monochloroacetic acid esters (1:2 ratio) in different alcohols. These reactions are an exothermic process. The It was found that highest yields (78-86%) occurred at a temperature of 50-60°C most probably owing to non- side reactions.

Table 1. Effect of temperature on the yield of the reaction of pyridine with esters of monochloroacetic acid.

№	Tertiary amine	Esters of monochloroacetic acid	Temperature, ^{0}C	Yield, %
3	Pyridine	3-methyl-pentyl (-C_5H_{11})	30-40	75
			50-60	84
			80-90	74
4		Hexyl (-C_6H_{13})	30-40	66
			50-60	78
			80-90	70
8		Benzyl ($C_6H_5CH_2$-)	30-40	74
			50-60	86
			80-90	72

The reasons behin the optimal reaction temperature is following. As-well known, pyridine is a weaker base than aliphatic amines, requiring higher temperatures for quaternary salt formation. When the reaction temperature is settled for 50-60°C, reaction favored due pyridine's lower basic strength. On the other hand, yields decrease at temperatures above the optimal range due to decomposition of salts at elevated temperature. Table 2 shows molar ratio also impacts yield. Applying the different ratio, , the 1:2 pyridine:ester ratio produced highest yields of 76-81%. In opposite site, stoichiometric ratio of (1:1) or

excess pyridine (1:1.5) ratio result in lower yields of 63-75%.. In conclusion, temperature of 50-60°C and molar ratio 1:2 were found to be optimal conditions to produce the highest yield of ionic liquid

Table 2. Influence of molar ratios of reagents on the reaction yield of pyridine and monochloroacetic acid esters

№	Tertiary amine	Esters of monochloroacetic acid	Molar ratio	Yield, %
1	Pyridine	3-methyl-pentyl (-C_5H_{11})	1:1	63
			1:2	76
			1:1,5	68
2		Hexyl (-C_6H_{13})	1:1	68
			1:2	81
			1:1,5	75
4		Benzyl ($C_6H_5CH_2$-)	1:1	69
			1:2	77
			1:1,5	72

Table 3 provides the reaction time versus yield relations. Based on the table, increasing esters of monochloroacetic acid lowers yield likely due to partial salt solubility in excess pyridine. The highest k yield of 80-84% occurred at 3 hours across substrates. Shorter (2 hour) or longer (4 hour) reaction times lowered yields, indicating 3 hours allows full reaction before side reactions. Optimal 1:2 ratio and 3 hour reaction time identified to maximize isolated yields. Additional adjustments did not improve or lowered results. Careful control of both molar feed and timing is necessary to optimize formation of these quaternary ammonium salts.

Table 3. Effect of time on the reaction yield of pyridine esters and monochloroacetic acid.

№	Esters of monochloroacetic acid	Reaction Time, min	Yield, %
1	3-methyl-pentyl (-C_5H_{11})	2	74
		3	84
		4	76
2	Hexyl (-C_6H_{13})	2	74
		3	82
		4	77
4	Benzyl ($C_6H_5CH_2$-)	2	76
		3	80
		4	78

We further assessed the effect of the solvent on the reaction yield. . Table 4 lists the effects of various solvents on the reactivity of pyridine with various monochloroacetic acid esters. In comparison to solvents, ethanol provided the highest yields between 78–84%. Based on these results, optimal conditions were identified as a 1:2 molar ratio of reactants, a temperature of 60°C, a reaction time of 3 hours using ethanol as the solvent. Table 5 confirms applying these optimized parameters to reactions between pyridine, 3-methyl-pentyl, hexyl and benzyl esters resulted in high yields between 80-84%. To purify the products, the salts were recrystallized from ethanol after heating, carbon treatment and filtration. This process yielded pure white salts. The purity of each salt was then assessed using thin-layer chromatography. Further characterization included determining physical properties and investigating structure.

Table 4. Effect of solvents on the reaction yield of pyridine and monochloroacetic acid esters.

№	Esters of monochloroacetic acid	Solvents	Reaction Yield, %
3	3-methyl-pentyl (-C_5H_{11})	Ethyl acetate	68

		Ethanol	84
		Acetone	71
4	Hexyl (-C_6H_{13})	Ethyl acetate	72
		Ethanol	79
		Acetone	67
8	Benzyl ($C_6H_5CH_2$-)	Ethyl acetate	72
		Ethanol	78
		Acetone	69

Table 5. Optimal yield of pyridine reactions with monochloroacetic acid esters.

№	Tertiary amine	Esters of monochloroacetic acid	Solvent	Reaction Time	Temperature, ^{0}C	Molar ratios of reactants	Yield, %
3	Pyridine	3-methyl-pentyl (-C_5H_{11})	Ethyl alcohol	3	60	1:2	84
4		Hexyl (R= C_6H_{13})	Ethyl alcohol	3	60	1:2	80
8		Benzyl ($C_6H_5CH_2$-)	Ethyl alcohol	3	60	1:2	81

4. Experimental-biological activity

4.1. Growth-promoting activity (seed growth)

The biological activity of the novel quaternary ammonium salts was evaluated using standardized wheat and cucumber seed in the case of germination and growth assays. These assays aimed to determine the potential growth-promoting effects of the compounds (Table 6). Among the spectrum of test compounds evaluated, 1-(2-(Benzyloxy)-2-oxoethyl)pyridin-1-ium chloride exhibited the most notable and consistent enhancement of both wheat and cucumber growth when juxtaposed with control groups. This effect was distinctly characterized by a lucid dose-dependent response, with enhancements surpassing the 20% threshold discernible within the lower concentration range of 0.0001-0.001% for this specific compound. Furthermore, 1-(2-(Hexyloxy)-2-oxoethyl)pyridin-1-ium chloride exhibited a discernable albeit moderate capacity to stimulate cucumber growth, albeit primarily evident at select concentrations within the range tested. In stark contrast, 1-(2-(Isopentyloxy)-2-oxoethyl)pyridin-1-ium chloride evinced a potent inhibitory effect on growth at higher doses, although it approximated the control levels at the 0.0001% concentration. In summation, the benzyloxy derivative closely replicated the concentration-dependent activity profile of Floroxan, rendering it the most promising candidate for advancing plant development across a comprehensive array of assays. This preliminary dataset underscores the imperative for further dedicated investigations into the potential of this compound as an innate regulator of plant growth. A succinct summary of these pivotal findings may be encapsulated as follows: The observed biological activity trends were inherently linked to the structural attributes of the compounds under scrutiny. Notably, oxyalkyl chains of greater length, exemplified by hexyloxy and benzyloxy moieties, demonstrated a heightened propensity for enhancing plant growth, in contrast to their isopentyloxy counterparts, a phenomenon facilitating efficacious translocation processes. The presence of an aromatic benzyloxy moiety within the compound emerged as a significant advantage, intimating its pivotal role in facilitating interactions with plant systems. This pattern mirrors the behavior of Floroxan, which also integrates an aromatic domain within its molecular structure. Furthermore, it was ascertained that elevated doses of isopentyloxy translated into substantial growth inhibition, potentially attributed to an excess of lipophilicity leading to membrane disruptions. Consequently, it is patently clear that achieving an optimal balance in the lipophilic/hydrophilic character of the oxyalkyl chain, concomitant with a judicious emphasis on its hydrogen-bonding potential, stands out as a critical determinant governing the stimulation of plant development.

Table 6. Growth-promoting activity (seed growth) of quaternary ammonium salts conditionally determined in wheat and cucumber seeds.

Experiment variation	Rate of consumption, %	The size of the measured parts of seedlings			
		Root length, cm	%	Stem height, cm	%
Wheat germ					
Control	b/o	7,51		6,91	
Etalon Floroxan	0,00001	10,13	34,8	8,31	20,4
1-(2-(Hexyloxy)-2-oxoethyl)pyridin-1-ium chloride	0,1	3,52	-	4,76	-
	0,001	4,72	-	5,08	-
	0,0001	6,51	-	5,51	-
1-(2-(Benzyloxy)-2-oxoethyl)pyridin-1-ium chloride	0,1	8,44	12,3	7,26	5,0
	0,001	9,08	20,9	7,41	7,2
	0,0001	9,71	29,2	7,78	12,5
1-(2-(Isopentyloxy)-2-oxoethyl)pyridin-1-ium chloride	0,1	0,44	-	1,81	-
	0,001	1,22	-	2,2	-
	0,0001	6,34	-	6,8	-
Cucumber sprouts					
Control	b/o	7,04		4,14	
Etalon Floroxan	0,00001	9,22	30,9	5,61	35,5
1-(2-(Hexyloxy)-2-oxoethyl)pyridin-1-ium chloride	0,1	6,12	-	3,85	-
	0,001	7,13	-	4,05	-
	0,0001	7,56	7,03	4,71	13,7
1-(2-(Benzyloxy)-2-oxoethyl)pyridin-1-ium chloride	0,1	7,14	1,4	4,33	4,5
	0,001	7,23	2,6	4,74	14,4
	0,0001	8,88	26,1	5,02	21,2
1-(2-(Isopentyloxy)-2-oxoethyl)pyridin-1-ium chloride	0,1	0,82	-	1,43	-
	0,001	1,83	-	2,81	-
	0,0001	5,73	-	3,4	-

4.2. Herbicidal activity

The herbicidal activity of the novel quaternary ammonium salts was rigorously assessed through wheat and cucumber seed bioassays. The commercial herbicide standards, Fusilade and Stomp, exhibited the expected robust inhibition of plant growth, serving as exemplary positive controls (Table 7). Within this context, the bioassay results illuminated that 1-(2-(Isopentyloxy)-2-oxoethyl)pyridin-1-ium chloride demonstrated a potent herbicidal effect, significantly reducing root and stem length by more than 80% at higher doses for both plant species, thus aligning with the controls. This underscores its remarkable contact herbicidal properties. Moreover, 1-(2-(Hexyloxy)-2-oxoethyl)pyridin-1-ium chloride also inhibited growth in a dose-dependent manner, albeit to a lesser extent compared to its isopentyloxy counterpart. Conversely, 1-(2-(Benzyloxy)-2-oxoethyl)pyridin-1-ium chloride exerted negligible influence on plant development, even at the highest concentrations tested. This observation implies that the modification of the oxyalkyl substituent has the potential to finely modulate the herbicidal activity profile. The concise isopentyloxy chain, it appears, exerts pronounced disruption on plant cell functions, particularly affecting membranes, while the benzyloxy variant demonstrates a milder impact. It is evident that these quaternary ammonium salts, characterized by their cationic nitrogen functionality, facilitate herbicidal action by disrupting vital plant cell processes. The incorporation of the ester linkage enhances their uptake, whereas the nature of the oxyalkyl chain significantly influences lipophilicity and membrane interactions. Compounds bearing shorter, branched chains, such as isopentyloxy, exhibit heightened lipophilicity and potent herbicidal properties, likely attributable to nonspecific membrane damage. In contrast, those with longer, less branched chains, exemplified by hexyloxy and benzyloxy derivatives, display reduced lipophilicity and a greater degree of selectivity in their herbicidal activity. The benzyloxy derivative's lack of growth inhibition suggests specific target interactions, as opposed to broader membrane effects. The pursuit of structure-activity optimization

holds the promise of yielding natural herbicides tailored to target specialized biochemical pathways, facilitating precise and selective weed control. This elucidation of structure-based mechanisms of action serves as a guiding beacon for future modifications in this domain.

Table 7. Herbicidal activity of quaternary ammonium salts conditionally on wheat and cucumber seeds.

Experiment variation	Rate of consumption, %	The size of the measured parts of seedlings			
		Root length, cm	%	Поянинг баландли ги, см	Root length, cm
Wheat germ					
Control	b/o	7,51		6,91	
Etalon Fusilade super	2,0-4,0 l/hectare	0	100	0	100
	0,0001	7,96	5,9	6,03	12,8
1-(2-(Hexyloxy)-2-oxoethyl)pyridin-1-ium chloride	0,1	3,52	53,2	4,76	31,2
	0,001	4,72	37,2	5,08	26,5
	0,0001	6,51	13,4	5,51	20,3
1-(2-(Benzyloxy)-2-oxoethyl)pyridin-1-ium chloride	0,1	8,44	-	7,26	-
	0,001	9,08	-	7,41	-
	0,0001	9,71	-	7,78	-
1-(2-(Isopentyloxy)-2-oxoethyl)pyridin-1-ium chloride	0,1	0,44	94,1	1,81	93,0
	0,001	1,22	83,8	2,2	68,2
	0,0001	6,34	15,6	6,8	1,6
Cucumber sprouts					
Control	b/o	7,04		4,14	
Etalon Stomp	1,0-2,0 l/hectare	0,13	98,2	0	100
1-(2-(Hexyloxy)-2-oxoethyl)pyridin-1-ium chloride	0,1	6,12	13,1	3,85	7,1
	0,001	7,13	-	4,05	2,2
	0,0001	7,56	-	4,71	-
1-(2-(Benzyloxy)-2-oxoethyl)pyridin-1-ium chloride	0,1	7,14	-	4,33	-
	0,001	7,23	-	4,74	-
	0,0001	8,88	-	5,02	-
1-(2-(Isopentyloxy)-2-oxoethyl)pyridin-1-ium chloride	0,1	0,82	88,0	1,43	65,5
	0,001	1,83	74,1	2,81	32,2
	0,0001	5,73	18,7	3,4	17,9

4.3. Insecticidal activity

The potential insecticidal properties of the novel quaternary ammonium salts were meticulously evaluated against C. maculatus pests. In preliminary screening assays, conducted at a 1% treatment concentration, all test compounds exhibited high mortality rates within a mere 24-hour timeframe, rivalling the performance of the commercial standard BAGIRA (Table 8). Notably, 1-(2-(Hexyloxy)-2-oxoethyl)pyridin-1-ium chloride emerged as the most efficacious, achieving an impressive kill rate of 92.5%. This result suggests a relatively robust insecticidal activity within the series. Predictably, pest mortality exhibited a concentration-dependent decline at lower dosage levels. Remarkably, both the benzyloxy and hexyloxy derivatives retained substantial pesticidal efficacy even at reduced concentrations ranging from 0.1% to 0.01%, underscoring their versatility within an effective dose range. This preliminary assessment underscores the potential of these novel quaternary ammonium compounds as promising candidates for natural insect control agents. It is evident that their toxicological impact is contingent upon both concentration and the specific oxyalkyl substituents employed, thereby providing invaluable guidance for forthcoming lead optimization endeavors. Consequently, further targeted investigations are warranted to validate their utility as biodegradable alternatives for insect control. The quaternary ammonium salts, characterized by their cationic nitrogen moieties, facilitate interactions with insect cell membranes and

organelles. The presence of lipophilic ester and oxyalkyl domains serves to enhance cuticle penetration and partitioning. The incorporation of more branched and shorter chains, exemplified by isopentyloxy, imparts heightened lipophilicity, potentially resulting in nonspecific membrane disruption. Conversely, longer linear chains, as observed in hexyloxy derivatives, and the introduction of aromatic groups, such as benzyloxy, may afford selectivity in targeting ion channels and receptors. This lends credence to the likelihood of multiple toxicity mechanisms, encompassing both membrane disruption and receptor-mediated effects. The realization that structure optimization could yield compounds tailored to target essential physiological systems further underscores the potential of these compounds as natural pesticides. The structure-activity data gleaned from this investigation provide key insights into the intricate mechanisms underpinning membrane and target-based insecticidal activity, thereby serving as a compass to navigate future analog design efforts in the realm of natural pesticide development.

Table 8. Determination of the mortality rate of *C. maculates* pests under the influence of substances quaternary ammonium salts.

Experiment variation	Concentration, %	Mortality rate, % in 24 hours
1-(2-(Benzyloxy)-2-oxoethyl)pyridin-1-ium chloride	1	88,0±0,05
	0,1	65,4±0,14
	0,01	30,5±0,10
1-(2-(Isopentyloxy)-2-oxoethyl)pyridin-1-ium chloride	1	48,6±0,16
	0,1	15,1±0,18
	0,01	7,3±0,11
1-(2-(Hexyloxy)-2-oxoethyl)pyridin-1-ium chloride	1	92,5±0,06
	0,1	83,7±0,08
	0,01	55,2±0,08
BAGIRA	0,1	87,0±0,05
	0,01	86,2±0,11
Control	b/o	3,7±0,04

5. Computational analysis

5.1. Density functional analysis

Calculated reactivity descriptors of three molecules are presented in Table 9. Optimized geometries, directions of the dipole moments, frontier molecular orbitals and distributions of the electrostatic potential are shown in Figures 2-4 in details. The HOMO molecular orbitals are localized on ligands, while the LUMO orbitals are localized mainly on C_5N rings. Therefore, all three molecules are characterized by almost the same LUMO orbital energies, and the difference in their electronic properties is determined by HOMO orbitals. HOMO energies slightly grow in a series of molecules 1-(2-(isopentyloxy)-2-oxoethyl)pyridin-1-ium, 1-(2-(hexyloxy)-2-oxoethyl)pyridin-1-ium and 1-(2-(benzyloxy)-2-oxoethyl)pyridin-1-ium. This growth is accompanied by a decrease in chemical rigidity and stability. However, the values of all quantum descriptors for all three molecules are almost the same. Figure 5 shows the total and partial densities of the electronic states of three molecules. One can see that carbon atoms provide major contributions to both frontier orbitals of each molecule.

Table 9. Calculated energies of frontier molecular orbitals HOMO and LUMO, HOMO-LUMO gaps, dipole moments *D* and quantum descriptors of reactivity for three considered molecules. Dipole moments are presented excluding/including PCM surface charges, respectively.

	1-(2-(Isopentyloxy)-2-oxoethyl)pyridin-1-ium	1-(2-(Hexyloxy)-2-oxoethyl)pyridin-1-ium	1-(2-(Benzyloxy)-2-oxoethyl)pyridin-1-ium

HOMO, eV	-11.15	-10.67	-9.36
LUMO, eV	-6.46	-6.46	-6.42
gap, eV	4.69	4.21	2.94
D, Debye	10.34	13.10	10.82
IP, eV	11.87	11.49	10.47
EA, eV	3.82	3.82	3.79
χ, eV	7.84	7.66	7.13
μ, eV	-7.84	-7.66	-7.13
η, eV	4.02	3.84	3.34
S, eV^{-1}	0.12	0.13	0.15
ω, eV	7.64	7.64	7.62
ε, eV^{-1}	0.13	0.13	0.13
ω^{-}, eV	12.07	11.95	11.60
ω^{+}, eV	4.22	4.29	4.47

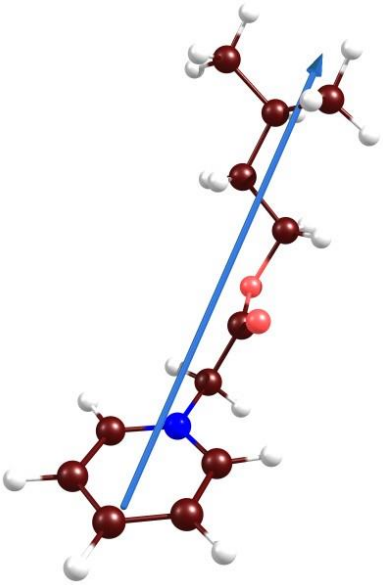

(a)

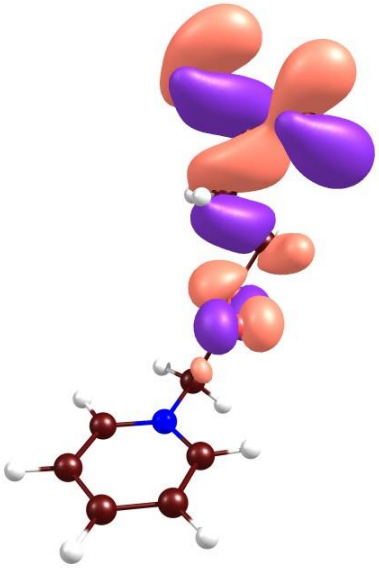

(b)

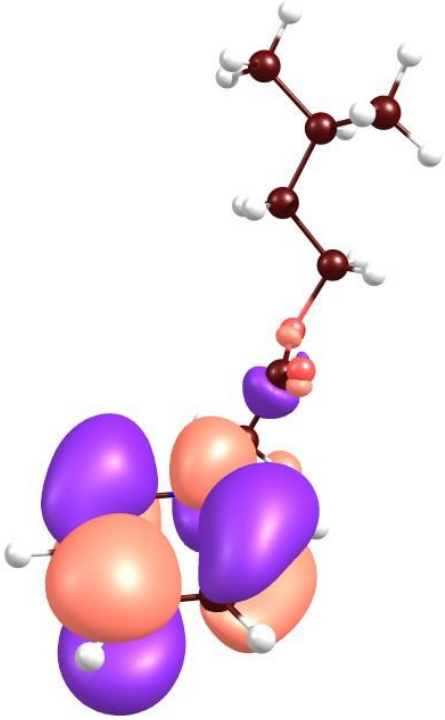

(c)

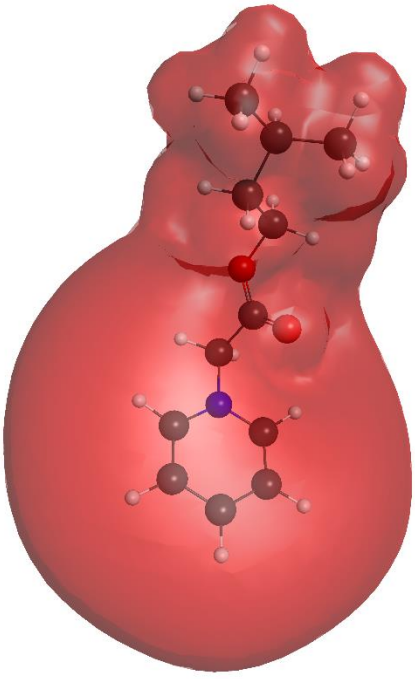

(d)

Figure 2. Structure (a), HOMO (b) and LUMO (c) frontier orbitals and electrostatic potential (d) of 1-(2-(Isopentyloxy)-2-oxoethyl)pyridin-1-ium. The blue arrow indicates the direction of the dipole moment. Brown, white, blue and red balls represent carbon, hydrogen, nitrogen and oxygen atoms, respectively.

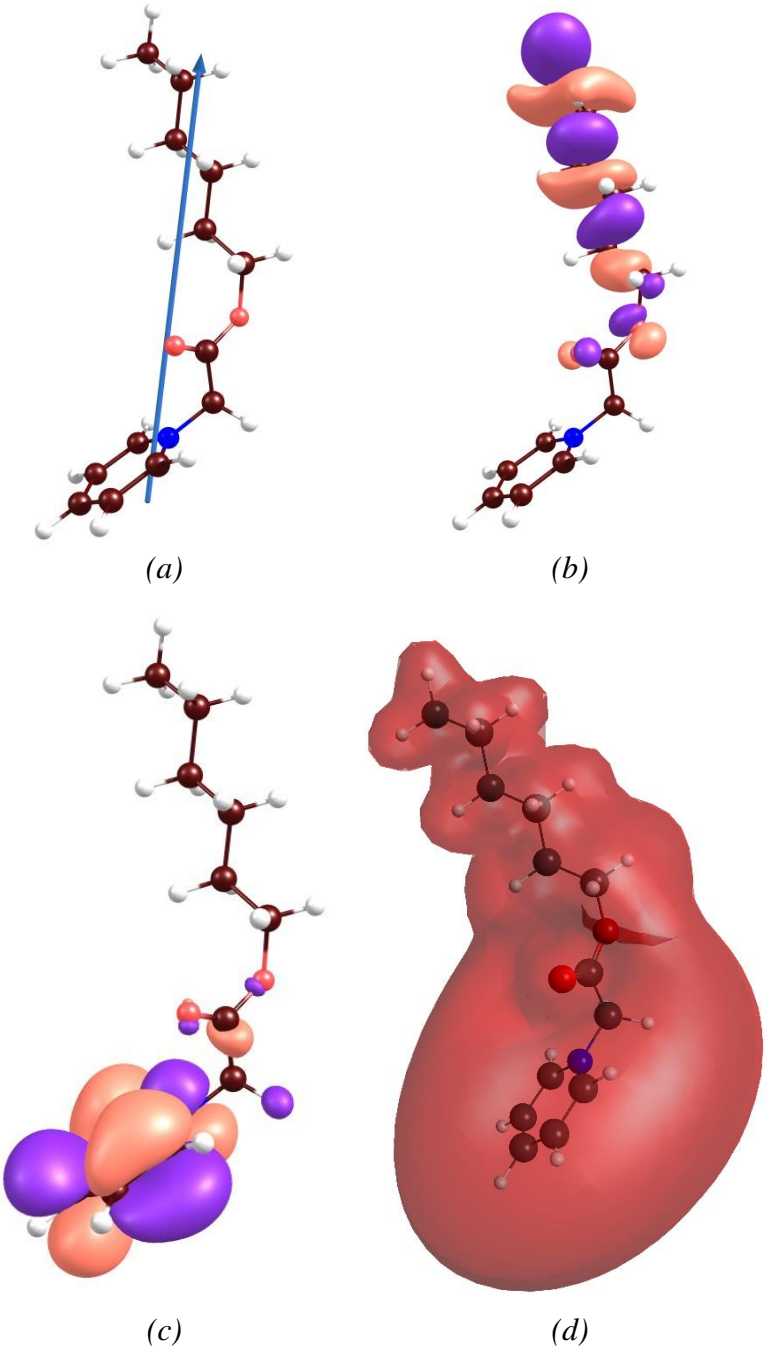

Figure 3. Structure (a), HOMO (b) and LUMO (c) frontier orbitals and electrostatic potential (d) of 1-(2-(Hexyloxy)-2-oxoethyl)pyridin-1-ium. The blue arrow indicates the direction of the dipole moment. Brown, white, blue and red balls represent carbon, hydrogen, nitrogen and oxygen atoms, respectively.

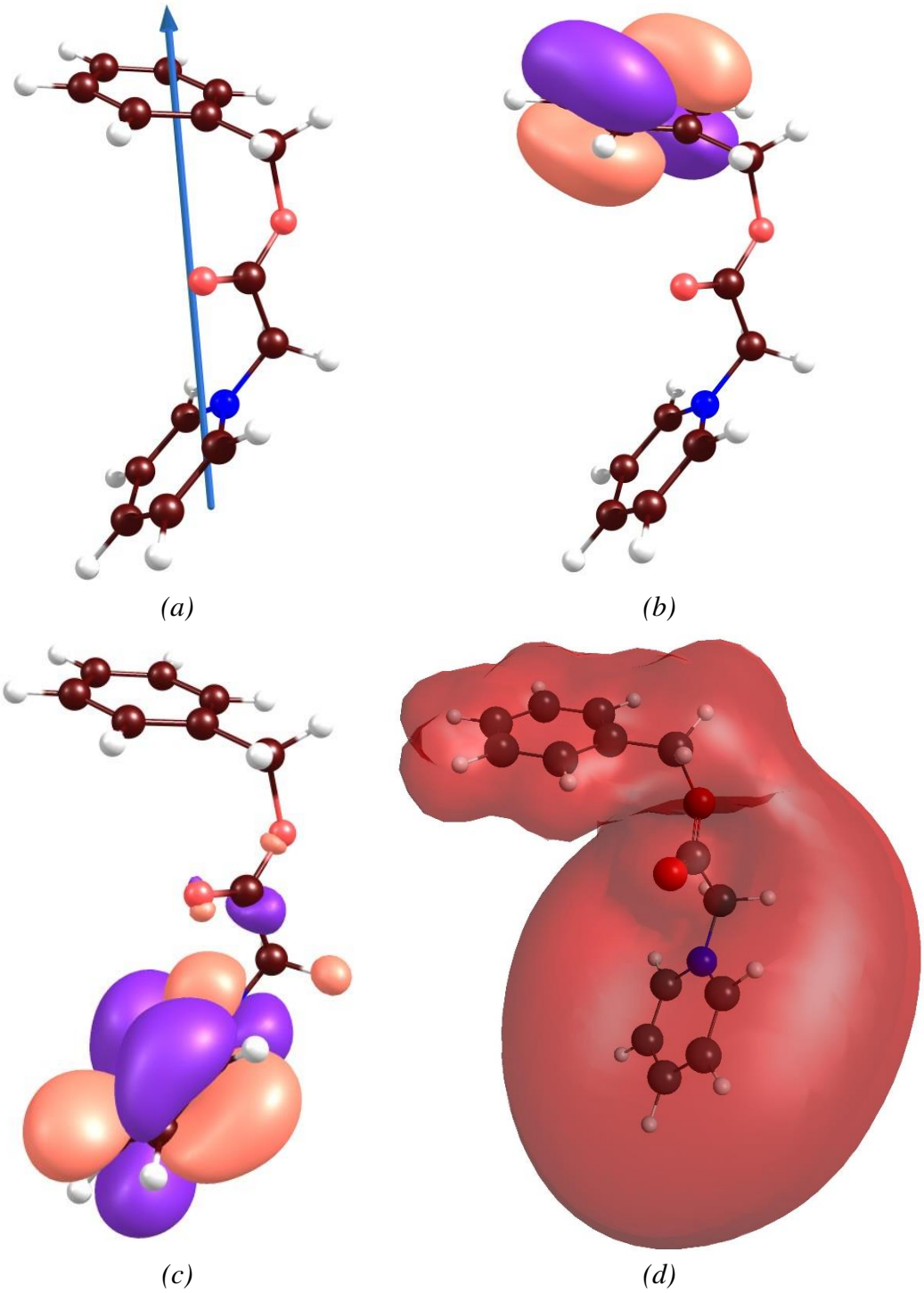

Figure 4. Structure (a), HOMO (b) and LUMO (c) frontier orbitals and electrostatic potential (d) of 1-(2-(Benzyloxy)-2-oxoethyl)pyridin-1-ium. The blue arrow indicates the direction of the dipole moment. Brown, white, blue and red balls represent carbon, hydrogen, nitrogen and oxygen atoms, respectively.

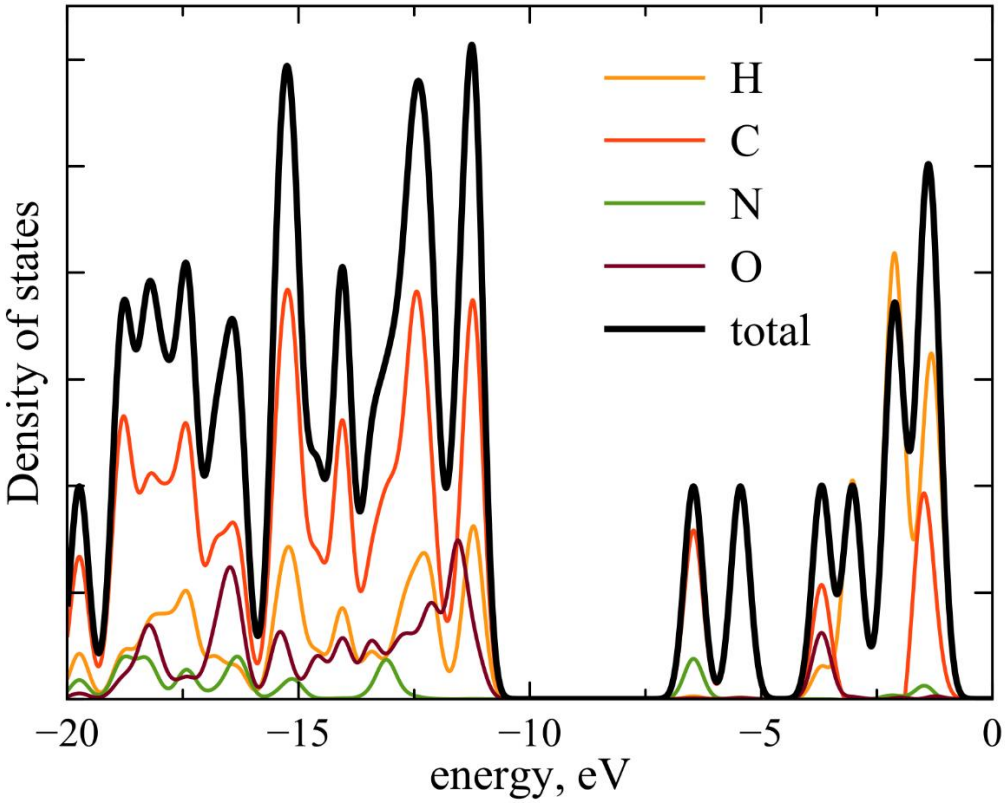
H
C
N
O
total
Density of states
−20
−15
−10
−5
0
energy, eV

(a)

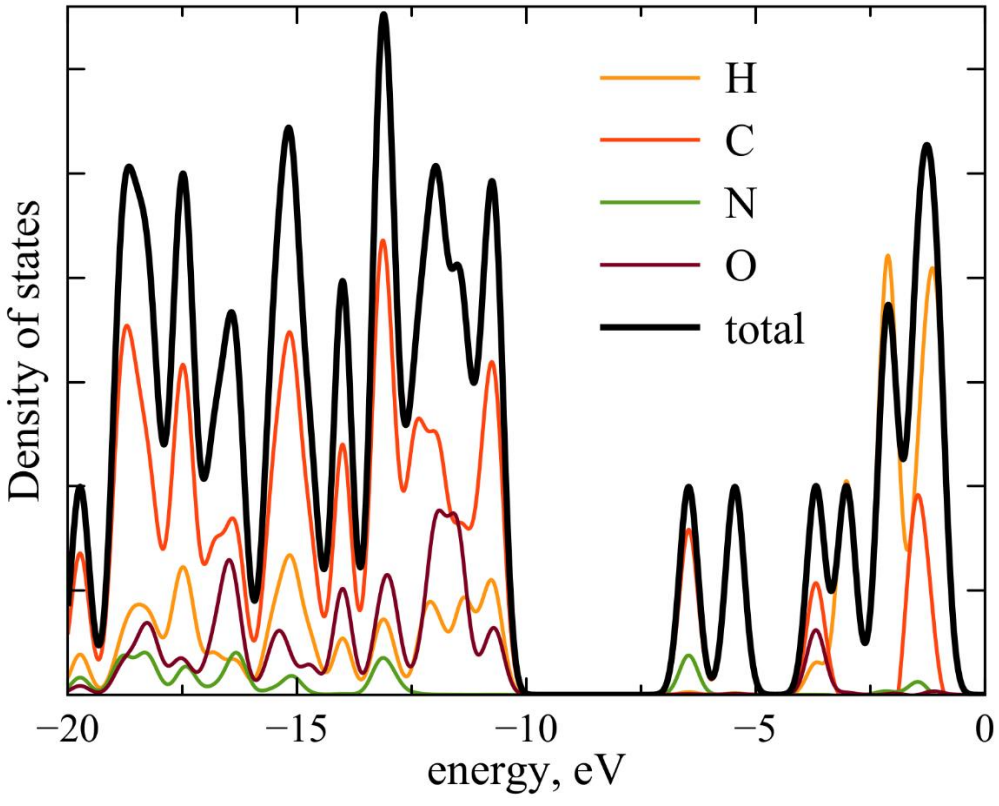
H
C
N
O
total
Density of states
−20
−15
−10
−5
0
energy, eV

(b)

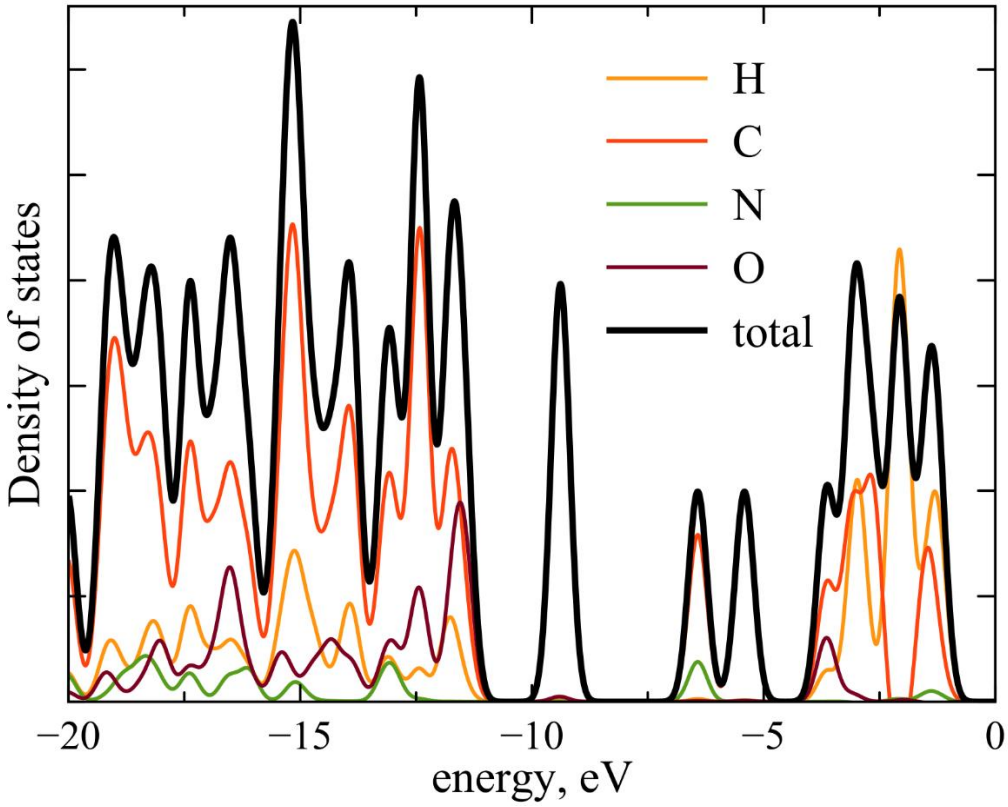

(c)

Figure 5. Total and partial densities of electronic states for the 1-(2-(Isopentyloxy)-2-oxoethyl)pyridin-1-ium (a), 1-(2-(Hexyloxy)-2-oxoethyl)pyridin-1-ium (b) and 1-(2-(Benzyloxy)-2-oxoethyl)pyridin-1-ium (c). The peaks of the density of states are broadened by Gaussians with $\sigma = 0.2$ eV.

5.2. Molecular docking analysis

For molecular docking analysis, we chose some proteins related to different kinds of cancers. We considered the following protein: 1JNX (relevant to breast cancer [41]), 6V9C (relevant to liver cancer [42]) and 1X2J (relevant to lung cancer [43]). Structures of these proteins and docking sites for selected compounds are shown in Figures 6, 7 and 8, respectively. The values of *VS* and K_a are collected in Table 10. One can see that all three molecules dock to the same cavities on the proteins (the only exception is the docking of 1-(2-(Hexyloxy)-2-oxoethyl)pyridin-1-ium on 1JNX). 1-(2-(Benzyloxy)-2-oxoethyl)pyridin-1-ium contained two hexagonal rings possesses the highest negative value of *VS*. Therefore, this molecule is the most biologically active. According to Table 10, 1-(2-(Benzyloxy)-2-oxoethyl)pyridin-1-ium docks more strongly to 1X2J than to other proteins under consideration.

Table 10. Calculated molecular docking parameters of three considered molecules on some cancer-related proteins.

	VS, kcal/mol	K_a, M^{-1}	Cavity volume, $Å^3$	Interacted fragments
1JNX (breast cancer)				
1-(2-(Isopentyloxy)-2-oxoethyl)pyridin-1-ium	-4.54	$1.5 \cdot 10^3$	94	N1678; L1679; I1680; T1681; E1682; L1701; K1702; L1705; Q1779; T1681; W1782
1-(2-(Hexyloxy)-2-oxoethyl)pyridin-1-ium	-4.20	$0.9 \cdot 10^3$	74	V1810; Q1811; P1812; D1813; T1834; R1835; E1836; T1852; Y1853; L1854; I1855
1-(2-(Benzyloxy)-2-oxoethyl)pyridin-1-ium	-5.54	$7.5 \cdot 10^3$	94	L1679; I1680; T1681; E1682; L1701; K1702; L1705; D1778; Q1779; W1782
6V9C (liver cancer)				
1-(2-(Isopentyloxy)-2-oxoethyl)pyridin-1-ium	-5.23	$4.6 \cdot 10^3$	809	L473; G474; V481; A501; K503; I534; V548; V550; I534; L619; A629
1-(2-(Hexyloxy)-2-	-4.93	$2.8 \cdot 10^3$	809	L473; V481; A501; K503; V548; E520;

oxoethyl)pyridin-1-ium				M524; C552; A553; A629; D630
1-(2-(Benzyloxy)-2-oxoethyl)pyridin-1-ium	-5.33	$5.3 \cdot 10^3$	809	G474; E475; V481; A501; K503; E520; V550; M524; I534; L619; D630
1X2J (lung cancer)				
1-(2-(Isopentyloxy)-2-oxoethyl)pyridin-1-ium	-5.52	$7.3 \cdot 10^3$	1166	L365; G367; V463; G464; V465; G509; A510; G511; V512; A556; L557
1-(2-(Hexyloxy)-2-oxoethyl)pyridin-1-ium	-5.52	$7.3 \cdot 10^3$	1166	A366; G367; V418; G464; V465; A466; C513; V514; I559; G605; V606
1-(2-(Benzyloxy)-2-oxoethyl)pyridin-1-ium	-6.32	$2.6 \cdot 10^4$	1166	L365; A366; G367; G464; V465; G511; V512; I416; G417; V418; L557; G558

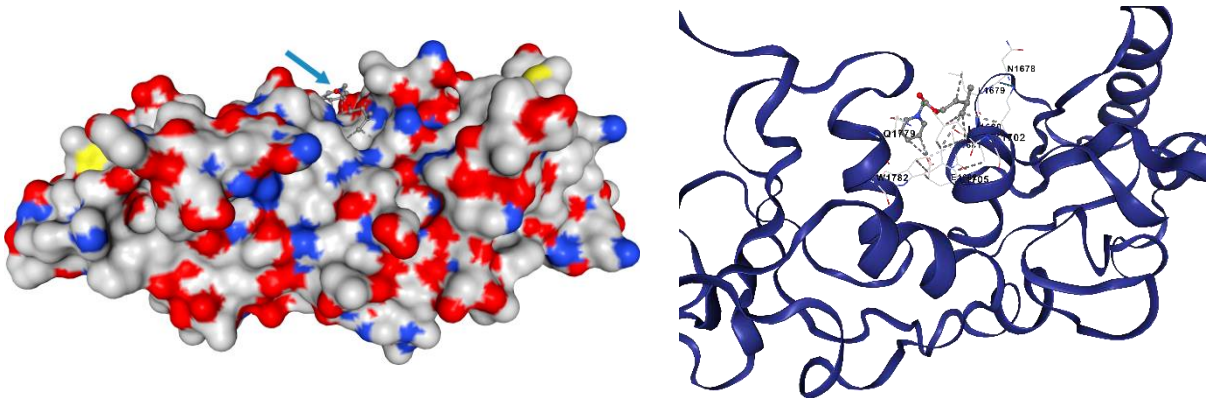

(a)

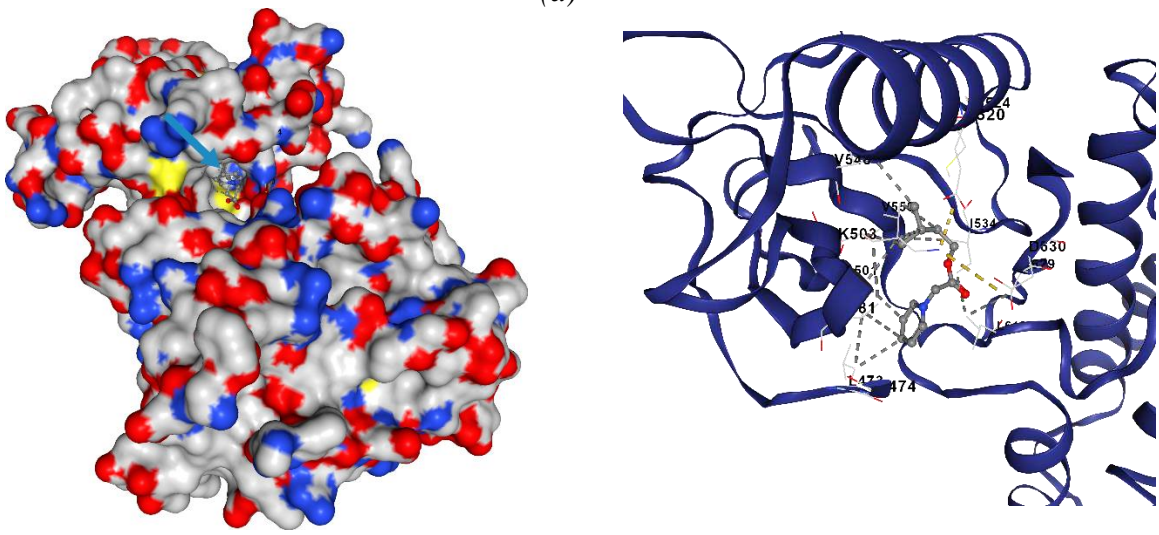

(b)

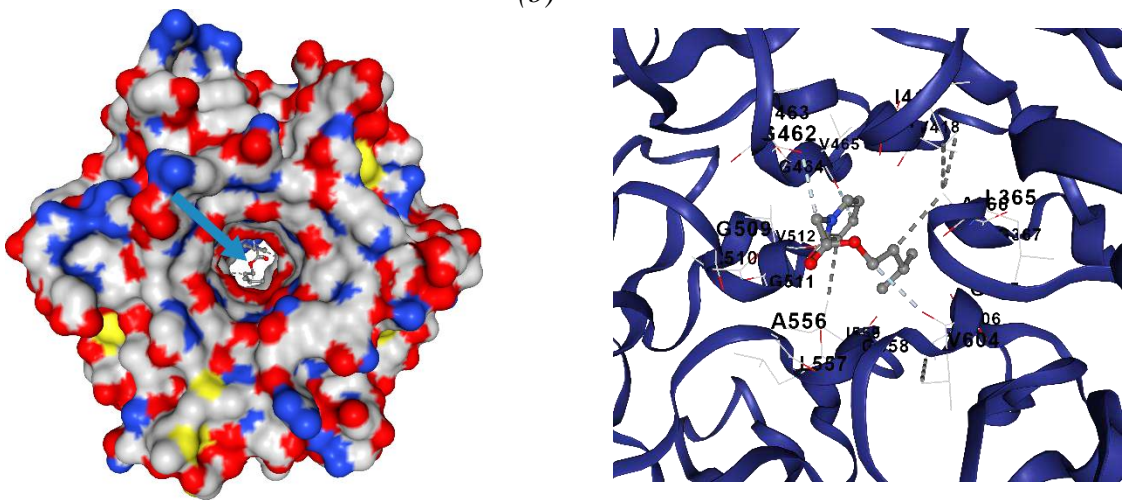

(c)

Figure 6. The best docking site for 1-(2-(Isopentyloxy)-2-oxoethyl)pyridin-1-ium attached to 1JNX (a), 6V9C (b) and 1X2J (c) proteins. General view (left) and detailed view of interacted region (right) are both presented for each protein. The blue arrows indicate the docking molecule.

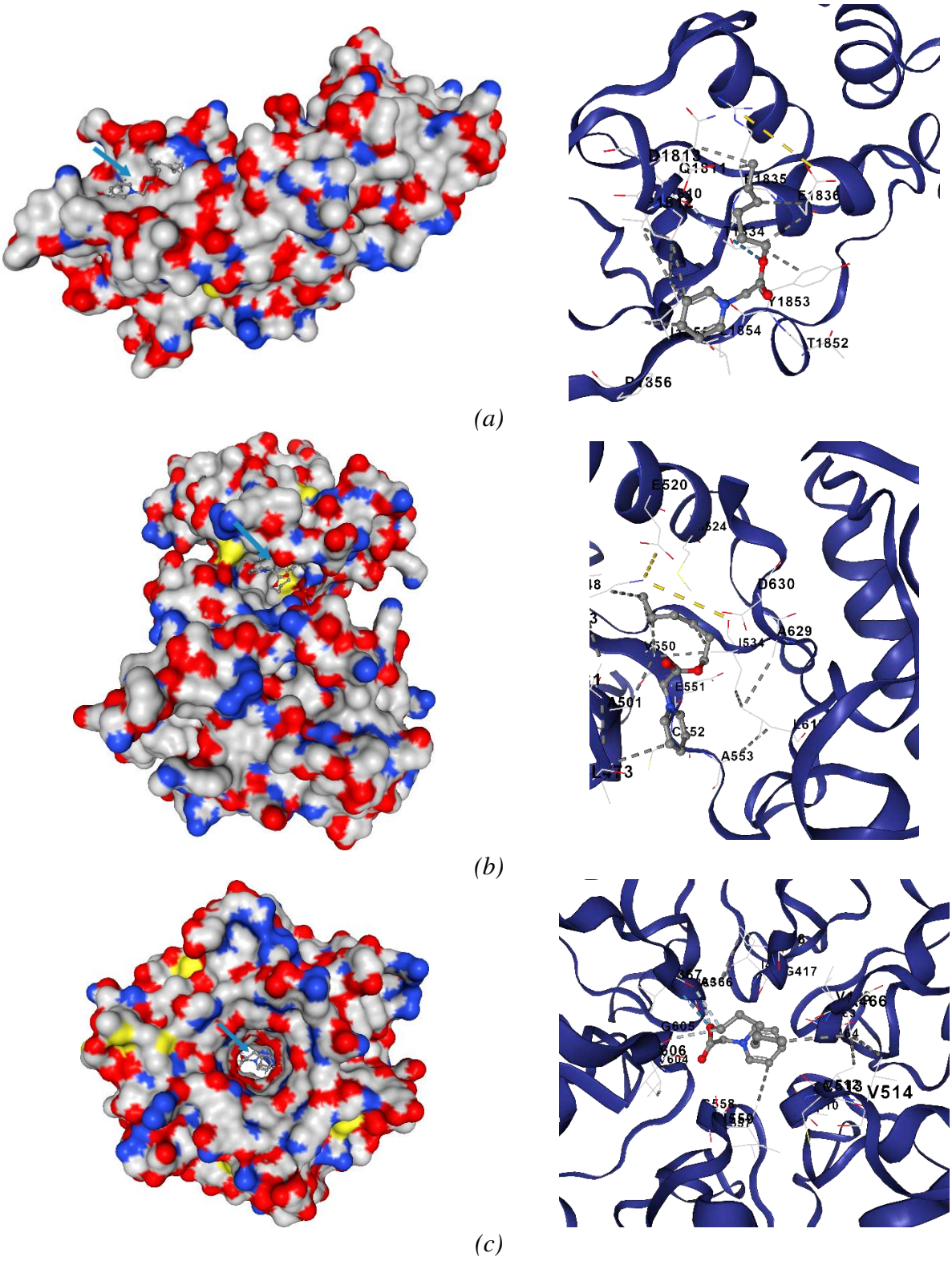

(a)

(b)

(c)

Figure 7. The best docking site for 1-(2-(Hexyloxy)-2-oxoethyl)pyridin-1-ium attached to 1JNX (a), 6V9C (b) and 1X2J (c) proteins. General view (left) and detailed view of interacted region (right) are both presented for each protein. The blue arrows indicate the docking molecule.

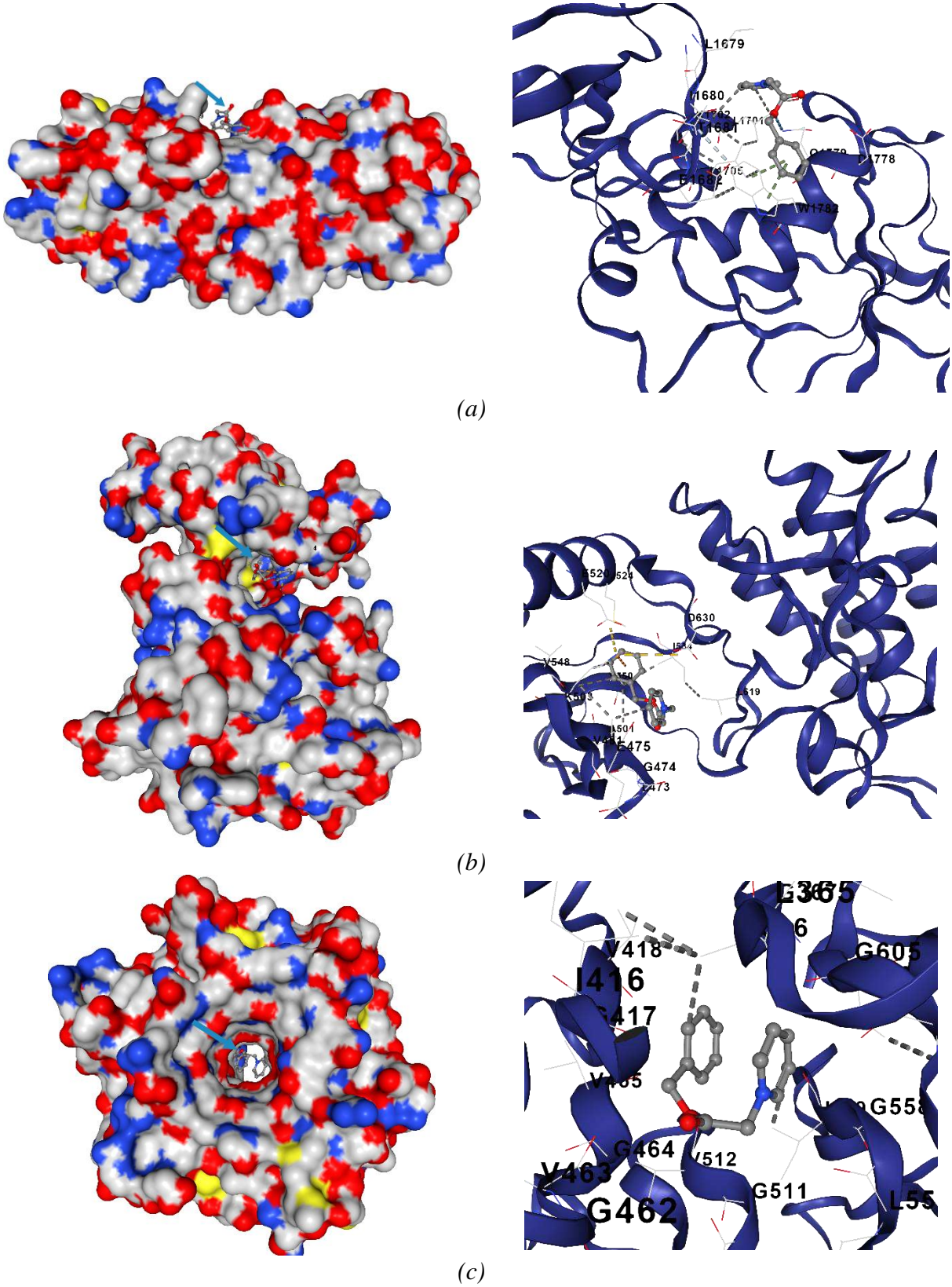

Figure 8. The best docking site for 1-(2-(Benzyloxy)-2-oxoethyl)pyridin-1-ium attached to 1JNX (a), 6V9C (b) and 1X2J (c) proteins. General view (left) and detailed view of interacted region (right) are both presented for each protein. The blue arrows indicate the docking molecule.

5.3. Petra/Osiris/Molinspiration (POM) analysis

Petra analysis provides prediction of some physical and chemical properties of organic molecules, including bonds dissociation enthalpies (BDE) and free energies (BDFE). However, novel approaches based on machine learning (ML) possesses higher accuracy of these values. This is why we apply one of such modern ML techniques [44] to estimate the BDE and BDFE of considered molecules. The results are

presented in Table 11. According to the data obtained, the C-N bonds are the weakest in all three molecules. BDE and BDFE values corresponding to these bonds are almost the same and equal to 60 and 47 kcal/mol, respectively. Therefore, the molecules are quite stable and do not dissociate under normal conditions.

Osiris analysis was performed with the OSIRIS Property Explorer. Obtained data are presented in Table 12. The *cLogP* value shows the logarithm of the ratio of solubility of the selected molecule in *n*-octanol and water. Lower values of *cLogP* correspond to higher hydrophilicity. All considered molecules possess $cLogP < 5$, and therefore their adsorption and permission characteristics should be regarded as acceptable. The *logS* characteristic is the logarithm of aqueous solubility of the molecule expressed in the mol/L units. Most drugs possess $logS > -4$; all three molecules also satisfy this condition. The value of *DL* is a measure of similarities between considered molecule and commonly known drugs. Fragments, which are usual for drugs, identified in considered molecules as well as their contributions to *DL* values are shown in Figure 9. One can see that only 1-(2-(Isopentyloxy)-2-oxoethyl)pyridin-1-ium demonstrates positively value of *DL*. Therefore, this molecule is more similar to drug then to non-drug chemical compounds. Toxicity risks were evaluated by the empirical methods implied in OSIRIS Property Explorer (see Table 12). Based on all parameters mentioned above, the values of drug score (*DS*) were calculated. The molecule 3 is the most safe and possesses the highest value of $DS = 0.47$.

Molinspiration analysis revealed the activity of considered molecules to common human receptors such as such as GPCRs, ion channels, kinases, nuclear receptors, proteases and enzymes [45]. The Molinspiration scores calculated with the software [46] are presented in Table 13. One can see that the molecules demonstrate very different bioactivities against different human receptors (see Table 13).

Table 11. The weakest interatomic bonds detected in the considered molecules and calculated corresponding BDE (kcal/mol) and BDFE (kcal/mol) values.

bond	BDE	BDFE
1-(2-(Isopentyloxy)-2-oxoethyl)pyridin-1-ium		
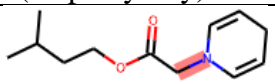	60.1	47.4
	68.1	59.9
	79.5	71.5
	82.5	69.1
1-(2-(Hexyloxy)-2-oxoethyl)pyridin-1-ium		
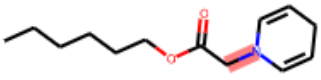	60.1	47.4
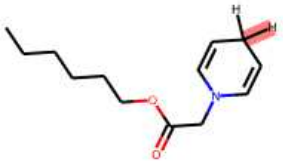	68.1	59.9
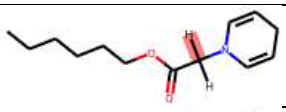	79.5	71.5
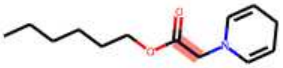	82.5	69.1
1-(2-(Benzyloxy)-2-oxoethyl)pyridin-1-ium		
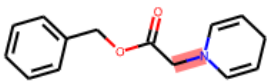	60.1	47.3

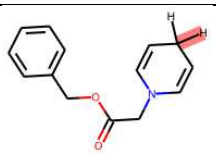	68.1	59.9
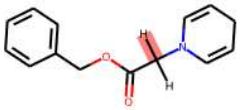	79.5	71.5
	81.7	68.3

Table 12. OSIRIS characteristics of considered molecules: hydrophilicity-based characteristic *cLogP*, aqueous solubility *logS*, total polar surface area *TPSA*, druglikeness *DL* and total drug score *DS*. Estimated mutagenicity/tumorigenicity/irritating/reproductive risks are also listed.

	cLogP	*logS*	*TPSA*	*DL*	*DS*	Toxicity risks
1-(2-(Isopentyloxy)-2-oxoethyl)pyridin-1-ium	1.55	-2.11	29.54	0.24	0.35	No/No/Medium/High
1-(2-(Hexyloxy)-2-oxoethyl)pyridin-1-ium	2.24	-2.49	29.54	-13.79	0.28	No/No/High/No
1-(2-(Benzyloxy)-2-oxoethyl)pyridin-1-ium	1.44	-2.44	29.54	-11.79	0.47	No/No/No/No

Table 13. Molinspiration scores of considered molecules against GPCR ligand (*GPCR*), ion channel modulator (*ICM*), kinase inhibitor (*KI*), nuclear receptor ligand (*NRL*), protease (*PI*) and enzyme inhibitors (*EI*).

	GPCR	*ICM*	*KI*	*NRL*	*PI*	*EI*
1-(2-(Isopentyloxy)-2-oxoethyl)pyridin-1-ium	-0.22	-0.03	-0.85	-0.59	-0.33	-0.02
1-(2-(Hexyloxy)-2-oxoethyl)pyridin-1-ium	-0.11	-0.02	-0.70	-0.44	-0.32	0.09
1-(2-(Benzyloxy)-2-oxoethyl)pyridin-1-ium	-0.03	0.09	-0.56	-0.40	-0.15	0.13

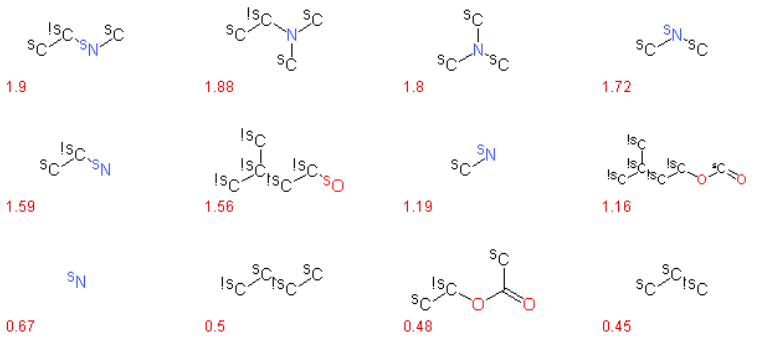

(a)

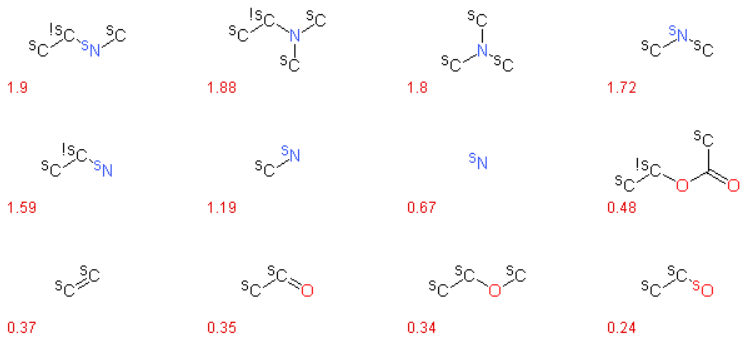

(b)

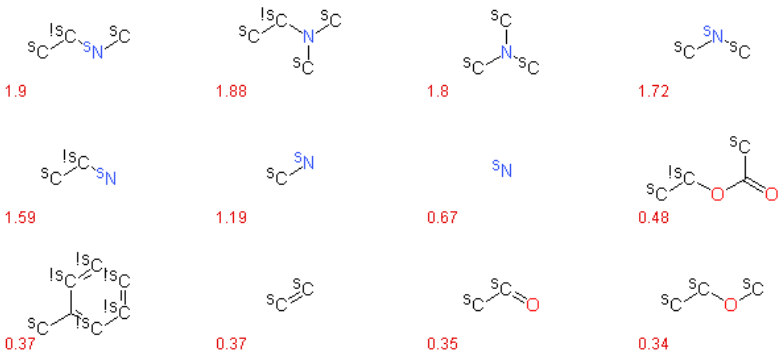

(c)

Figure 9. Drugs-like fragments of the considered molecules 1-(2-(Isopentyloxy)-2-oxoethyl)pyridin-1-ium (a), 1-(2-(Hexyloxy)-2-oxoethyl)pyridin-1-ium (b) and 1-(2-(Benzyloxy)-2-oxoethyl)pyridin-1-ium (c) as well as their contributions to corresponding *DL* values relevant to OSIRIS analysis.

6. Estimated application

It was found some potential applications that could be estimated from this study:

Agricultural Applications:

- The lead compounds, particularly the benzyloxy derivative, show promise as natural plant growth regulators/fertilizers to promote crop yields.
- The isopentyloxy salt's potent herbicidal activity indicates applications as a biopesticide for selective weed control in organic farming.
- With further optimization guided by the SAR knowledge, these pyridinium ILs could replace conventional toxic agrochemicals.

Pharmaceutical Applications:

- The high predicted bioactivities and docking affinities to cancer proteins suggest potential as anti-cancer lead compounds.
- Further development may yield IL-based drugs targeting diseases like breast, liver or lung cancers.
- Optimization targeting specific receptors/ion channels could produce medication with improved selectivity over current therapies.

Industrial Applications:

- The insecticidal properties open up uses as natural biodegradable pest control agents for agriculture/households.
- Additional structural tuning may deliver IL insecticides/miticides effective against key agricultural/storage pests.
- Other applications are possible as antimicrobial agents, functional materials, separation/extraction solvents leveraging their tunable properties.

Commercialization:

- With more rigorous in vivo efficacy/toxicity testing, some lead compounds could potentially reach clinical trials or market within 5-10 years.
- Others may enter commercial use sooner as natural pesticides, fertilizers or antimicrobial formulations requiring less extensive development.
- Global markets for agrochemicals, pharmaceuticals and industrial biocides worth billions provide commercial opportunities.

7. Conclusion

The following main conclusions were found:

- Three novel pyridinium ionic liquids were successfully synthesized and characterized.
- Reaction conditions were optimized to yield the pure quaternary ammonium salts in good yields up to 86%.
- The benzyloxy derivative showed the strongest plant growth promotion effects in a dose-dependent manner.

- The isopentyloxy compound inhibited root and shoot growth the most potently in herbicide assays.
- All structures exhibited significant insecticidal activity versus controls.
- Electronic properties, reactivities and frontier orbital distributions were calculated using DFT methods.
- Molecular docking revealed favorable binding interactions and affinities at cancer protein targets.
- The benzyloxy ionic liquid emerged as the most active lead based on computational predictions.
- Activity profiles depended systematically on ester substituent chain length and structure.
- Shorter, more lipophilic chains conferred stronger herbicidal action through membrane impacts.
- Longer, less lipophilic chains and aromatic groups enhanced selectivity via specific target interactions.
- Combining experiments and modeling provided a comprehensive SAR understanding.
- Insights into mechanisms guide rational design of more optimized compounds.
- Findings support further targeted syntheses focused on agricultural and pharmaceutical profiles.
- This integrated approach establishes a pathway to functional discovery of sustainable bioactive leads.

Declaration of interests

The authors declare that they have no known competing financial interests or personal relationships that could have appeared to influence the work reported in this paper.

Reference

1. Alrefaee, S.H., *Effect of alkyl chain length and halide ions on the corrosion inhibition potential of imidazolium and pyridinium based ionic liquids: computational studies.* Journal of Molecular Liquids, 2021. **344**: p. 117848.
2. Al-Sodies, S.A., et al., *Microwave and conventional synthesis of ester based dicationic pyridinium ionic liquids carrying hydrazone linkage: DNA binding, anticancer and docking studies.* Journal of Molecular Structure, 2020. **1207**: p. 127756-127756.
3. Asim, A.M., M. Uroos, and N. Muhammad, *Extraction of lignin and quantitative sugar release from biomass using efficient and cost-effective pyridinium protic ionic liquids.* RSC advances, 2020. **10**(72): p. 44003-44014.
4. Asim, A.M., et al., *Pyridinium protic ionic liquids: Effective solvents for delignification of wheat straw.* Journal of Molecular Liquids, 2021. **325**: p. 115013.
5. Chen, H., et al., *The molecular behavior of pyridinium/imidazolium based ionic liquids and toluene binary systems.* Physical Chemistry Chemical Physics, 2021. **23**(23): p. 13300-13309.
6. Chen, X., et al., *Effects of pyridinium-based ionic liquids with different alkyl chain lengths on the growth of maize seedlings.* Journal of Hazardous Materials, 2022. **427**: p. 127868-127868.
7. Deimede, V., et al., *Pyridinium based Poly (Ionic Liquids) membranes with exceptional high water vapor permeability and selectivity.* Separation and Purification Technology, 2020. **251**: p. 117412-117412.
8. Delgado-Mellado, N., et al., *Ecotoxicity evaluation towards Vibrio fischeri of imidazolium-and pyridinium-based ionic liquids for their use in separation processes.* SN Applied Sciences, 2019. **1**: p. 1-9.
9. El-Hajjaji, F., et al., *Electrochemical and theoretical insights on the adsorption and corrosion inhibition of novel pyridinium-derived ionic liquids for mild steel in 1 M HCl.* Journal of Molecular Liquids, 2020. **314**: p. 113737.
10. Ezzat, A.O., H.A. Al-Lohedan, and A.M. Atta, *New amphiphilic tricationic imidazolium and pyridinium ionic liquids for demulsification of arabic heavy crude oil brine emulsions.* ACS omega, 2021. **6**(7): p. 5061-5073.
11. Ezzat, A.O., A.M. Atta, and H.A. Al-Lohedan, *Demulsification of stable seawater/Arabian heavy crude oil emulsions using star-like tricationic pyridinium ionic liquids.* Fuel, 2021. **304**: p. 121436.
12. Ezzat, A.O., A.M. Tawfeek, and H.A. Al-Lohedan, *Synthesis and application of novel gemini pyridinium ionic liquids as demulsifiers for arabian heavy crude oil emulsions.* Colloids and Surfaces A: Physicochemical and Engineering Aspects, 2022. **634**: p. 127961.

13. Garcia, M.T., et al., *Surface activity, self-aggregation and antimicrobial activity of catanionic mixtures of surface active imidazolium-or pyridinium-based ionic liquids and sodium bis (2-ethylhexyl) sulfosuccionate.* Journal of Molecular Liquids, 2020. **303**: p. 112637-112637.
14. Hajjaji, F.E., et al., *Pyridinium-based ionic liquids as novel eco-friendly corrosion inhibitors for mild steel in molar hydrochloric acid: Experimental & computational approach.* Surfaces and Interfaces, 2021. **22**: p. 100881.
15. Hu, K., et al., *Removal of aluminum to obtain high purity gadolinium with pyridinium-based ionic liquids.* Hydrometallurgy, 2022. **213**: p. 105930-105930.
16. Husain, A., et al., *Demulsification of heavy petroleum emulsion using pyridinium ionic liquids with distinct anion branching.* Energy & Fuels, 2021. **35**(20): p. 16527-16533.
17. Tamilarasan, R., et al., *Synthesis, characterization, pharmacogenomics, and molecular simulation of pyridinium type of ionic liquids and their applications.* ACS omega, 2023. **8**(4): p. 4146-4155.
18. Valeh-e-Sheyda, P., M.F. Masouleh, and P. Zarei-Kia, *Prediction of CO2 solubility in pyridinium-based ionic liquids implementing new descriptor-based chemoinformatics models.* Fluid Phase Equilibria, 2021. **546**: p. 113136-113136.
19. Wang, Y., et al., *Superlithiation Performance of Pyridinium Polymerized Ionic Liquids with Fast Li+ Diffusion Kinetics as Anode Materials for Lithium-Ion Battery.* Small, 2023: p. 2302811-2302811.
20. Zang, H., et al., *Valorization of chitin derived N-acetyl-D-glucosamine into high valuable N-containing 3-acetamido-5-acetylfuran using pyridinium-based ionic liquids.* Journal of Molecular Liquids, 2021. **330**: p. 115667-115667.
21. Hussain, S., et al., *Investigation uncovered the impact of anions on CO2 absorption by low viscous ether functionalized pyridinium ionic liquids.* Journal of Molecular Liquids, 2021. **336**: p. 116362.
22. Kazmi, B., et al., *Energy, exergy and economic (3E) evaluation of CO2 capture from natural gas using pyridinium functionalized ionic liquids: A simulation study.* Journal of Natural Gas Science and Engineering, 2021. **90**: p. 103951-103951.
23. Kurtoğlu-Öztulum, S.F., A. Jalal, and A. Uzun, *Thermal stability limits of imidazolium, piperidinium, pyridinium, and pyrrolidinium ionic liquids immobilized on metal oxides.* Journal of Molecular Liquids, 2022. **363**: p. 119804.
24. Singh, A., et al., *Evaluation of corrosion mitigation properties of pyridinium-based ionic liquids on carbon steel in 15% HCl under the hydrodynamic condition: Experimental, surface, and computational approaches.* Journal of Molecular Liquids, 2023. **376**: p. 121408-121408.
25. Mao, H., et al., *Structure-activity relationship toward electrocatalytic nitrogen reduction of MoS2 growing on polypyrrole/graphene oxide affected by pyridinium-type ionic liquids.* Chemical Engineering Journal, 2021. **425**: p. 131769.
26. Norouzi, F. and A. Abdolmaleki, *CO2 conversion into carbonate using pyridinium-based ionic liquids under mild conditions.* Fuel, 2023. **334**: p. 126641.
27. Pérez, S.A., et al., *In vitro cytotoxicity assessment of monocationic and dicationic pyridinium-based ionic liquids on HeLa, MCF-7, BGM and EA. hy926 cell lines.* Journal of hazardous materials, 2020. **385**: p. 121513.
28. Reiß, M., et al., *Synthesis of novel carbohydrate based pyridinium ionic liquids and cytotoxicity of ionic liquids for mammalian cells.* RSC advances, 2020. **10**(24): p. 14299-14304.
29. Suk, M. and K. Kümmerer, *Towards greener and sustainable ionic liquids using naturally occurring and nature-inspired pyridinium structures.* Green Chemistry, 2023. **25**(1): p. 365-374.
30. Lee, C., W. Yang, and R.G. Parr, *Development of the Colle-Salvetti correlation-energy formula into a functional of the electron density.* Physical review B, 1988. **37**(2): p. 785.
31. Becke, A., *Density-functional thermochemistry. III. The role of exact exchange (1993) J.* Chem. Phys. **98**: p. 5648.
32. Krishnan, R., et al., *Self-consistent molecular orbital methods. XX. A basis set for correlated wave functions.* The Journal of chemical physics, 1980. **72**(1): p. 650-654.
33. Grimme, S., S. Ehrlich, and L. Goerigk, *Effect of the damping function in dispersion corrected density functional theory.* Journal of computational chemistry, 2011. **32**(7): p. 1456-1465.
34. Schmidt, M.W., et al., *General atomic and molecular electronic structure system.* Journal of computational chemistry, 1993. **14**(11): p. 1347-1363.

35. Bondarev, N.V., et al., *Probing of Neural Networks as a Bridge from Ab Initio Relevant Characteristics to Differential Scanning Calorimetry Measurements of High-Energy Compounds.* physica status solidi (RRL)–Rapid Research Letters, 2022. **16**(3): p. 2100191.
36. Martínez-Araya, J.I., G. Salgado-Morán, and D. Glossman-Mitnik, *Computational Nanochemistry Report on the Oxicams Conceptual DFT Indices and Chemical Reactivity.* The Journal of Physical Chemistry B, 2013. **117**(21): p. 6339-6351.
37. Gimaldinova, M.A., M.M. Maslov, and K.P. Katin, *Electronic and reactivity characteristics of CL-20 covalent chains and networks: a density functional theory study.* CrystEngComm, 2018. **20**(30): p. 4336-4344.
38. Liu, Y., et al., *CB-Dock: A web server for cavity detection-guided protein–ligand blind docking.* Acta Pharmacologica Sinica, 2020. **41**(1): p. 138-144.
39. Vaezi, M., et al., *Thermodynamic, kinetic and docking studies of some unsaturated fatty acids-quercetin derivatives as inhibitors of mushroom tyrosinase.* AIMS Biophys, 2020. **7**(4): p. 393-410.
40. Rbaa, M., et al., *Synthesis, characterization and bioactivity of novel 8-hydroxyquinoline derivatives: Experimental, molecular docking, DFT and POM analyses.* Journal of Molecular Structure, 2022. **1258**: p. 132688.
41. Williams, R.S., R. Green, and J.N.M. Glover, *Crystal structure of the BRCT repeat region from the breast cancer-associated protein BRCA1.* Nature structural biology, 2001. **8**(10): p. 838-842.
42. Liu, H., et al., *Discovery of selective, covalent FGFR4 inhibitors with antitumor activity in models of hepatocellular carcinoma.* ACS Medicinal Chemistry Letters, 2020. **11**(10): p. 1899-1904.
43. Padmanabhan, B., et al., *Structural basis for defects of Keap1 activity provoked by its point mutations in lung cancer.* Molecular cell, 2006. **21**(5): p. 689-700.
44. St. John, P.C., et al., *Prediction of organic homolytic bond dissociation enthalpies at near chemical accuracy with sub-second computational cost.* Nature communications, 2020. **11**(1): p. 2328.
45. Proudfoot, J.R., *Drugs, leads, and drug-likeness: an analysis of some recently launched drugs.* Bioorganic & medicinal chemistry letters, 2002. **12**(12): p. 1647-1650.
46. Grob, S., *Molinspiration Cheminformatics Free Web Services*. 2021.

Supplementary Files

This is a list of supplementary files associated with this preprint. Click to download.

- Supportingdocuments3.09.2023.docx